PHYSICAL REVIEW D **89,** 104008 (2014)

Fermi normal coordinates and fermion curvature couplings in general relativity

Anshuman Dey,[*] Abhisek Samanta,[†] and Tapobrata Sarkar[‡]

Department of Physics, Indian Institute of Technology, Kanpur 208016, India

(Received 17 March 2014; published 5 May 2014)

We study gravitational curvature effects in circular and radial geodesics in static, spherically symmetric space-times, using Fermi normal coordinates. We first set up these coordinates in the general case, and then use this to study effective magnetic fields due to gravitational curvature in the exterior and interior Schwarzschild, Janis-Newman-Winicour, and Bertrand space-times. We show that these fields can be large for specific parameter values in the theories, and thus might have observational significance. We discuss the qualitative differences of the magnetic field for vacuum space-times and for those seeded by matter. We estimate the magnitude of these fields in realistic galactic scenarios and discuss their possible experimental relevance. Gravitational curvature corrections to the hydrogen atom spectrum for these space-times are also discussed briefly.

DOI: 10.1103/PhysRevD.89.104008 PACS numbers: 04.20.-q, 04.80.Cc, 95.30.Sf

I. INTRODUCTION

Einstein's general theory of relativity (GR) [1] is an established theory of gravity, and many experimental tests of this theory are well known. In particular, studying the effect of space-time curvature on spin systems has a long history (see, e.g., [2]) starting from the celebrated work of de Sitter almost a century back [3]. Indeed, recent experimental results from the Gravity Probe B experiment [4] have successfully demonstrated the geodetic and frame-dragging effects, further strengthening the basis of GR.

Another interesting direction of work has been the analysis of gravitational effects on elementary particles. For example, the Dirac equation was analyzed in general curved space-times by Parker [5–7], who calculated the shifts in the hydrogen atom spectra due to gravity. His results showed that, for example, at the surface of the Sun, the typical contribution of gravity effects will result in shifting the energy levels of the hydrogen atom to the order of 10^{-50} GeV, which is unfortunately too small to detect by present day experiments. Along these lines, one can also think of possible apparent violations of Lorentz and *CPT* invariance due to gravitational effects (see, e.g., [8]). These are not actual violations but arise due to gravitation, and can be detected by experiments. The EOT-Wash experiment [9] has been actively seeking to detect such effects via torsion balance measurements, and one of its objectives is to measure gravitational interactions that couple to the spin of elementary particles. Here, the effect of gravity on an individual spin is magnified by considering a balance consisting of a very large number of such spins, and bounds have been placed on magnetic fields that can arise due to gravitational effects.

Although a preliminary analysis of gravitational effects on particles show that these might be hard to detect with present day experiments [10], it is important and interesting to understand scenarios where these might be large. In fact, one might hope to understand qualitative features of space-time itself, by analyzing such large effects, if they exist. Naturally, gravitational effects should maximize near large gravitating bodies, and GR predictions of physical effects in this regime might be of interest in futuristic experiments. For example, a concrete question to ask is whether there is any observable enhancement of gravitational effects on spinors near a massive object like a black hole or a neutron star. Or, we could try to determine such effects near a Galactic center which is dominated by dark matter. There are two immediate problems that arise here. First, any such computation will be model dependent, and more important, a general relativistic prediction of a physical effect is observer dependent; one needs to take care of subtleties regarding the latter. There is ample literature on the subject (see, e.g., [11]) which deals with important phenomenological issues, and in this work we try to complement these by a more formal approach.

Consider an observer in free fall, i.e., in geodesic motion in a gravitational background. We assume that the motion does not backreact on the metric; i.e., our observer is treated as a test particle in a gravitational background. Now say our observer does an experiment on a spin system. By writing the Dirac Lagrangian appropriate to a curved background, one can show that this will have fermionic pseudovector couplings, which in the nonrelativistic limit reduce to an interaction energy of the form $\vec{s}.\vec{b}$ with $\vec{s}$ being the spin of the particle [8,12,13]. This is what our geodesic observer seeks to determine, perhaps with a torsion balance setup. To calculate the effective magnetic field $\vec{b}$ due to gravitational interactions (to be distinguished from the intrinsic magnetic

[*]deyanshu@iitk.ac.in
[†]rupam@iitk.ac.in
[‡]tapo@iitk.ac.in

field that arises due to motion of charged particles), we need to make a choice of the coordinate system. A natural choice, motivated from physical considerations is the Fermi normal coordinate system, first introduced by Manasse and Misner [14]. In Fermi normal coordinates, the metric is locally flat all along the geodesic; i.e., the Christoffel connections vanish everywhere on the geodesic, although its derivatives may not be zero. In this coordinate frame, our locally flat observer can measure an effective magnetic field acting on the spin of the particle. The advantage of using Fermi normal coordinates is that one can talk about measurements carried out close to a singularity and not necessarily in a weak field limit. We can therefore address the question of the effect of gravity when it is large (of course, possible quantum gravity corrections are ignored). Although the implications of such measurements in present day experiments are far from obvious, it might encode valuable insights into the nature of space-time.

In this paper, we carry out such an analysis of observers in circular and radial geodesic motion for the Schwarzschild, Janis-Newman-Winicour (JNW) and Bertrand space-times. While the former is a vacuum solution of gravity, JNW space-times are sourced by a scalar field that satisfies the Einstein-Klein-Gordon equations and the Bertrand space-times (BSTs) are seeded by matter that can be given an effective two-fluid description [15,16] and can be thought of as a candidate for galactic dark matter. We highlight the important differences between the nature of gravitational couplings on fermions in these space-times and show that for Schwarzschild, JNW and BST backgrounds, such couplings can be large on highly relativistic orbits. For BST backgrounds, our results indicate that it might be possible to obtain indications of galactic dark matter in futuristic experiments.

This paper is organized as follows. In the next section, after briefly reviewing aspects of general spherically symmetric metrics in Fermi normal coordinates, we analyze observers in circular geodesic motion and calculate the effective magnetic field due to curvature couplings in Schwarzschild, JNW and BST backgrounds. In Sec. 3, we follow up this analysis for radial motion in the same backgrounds. We comment on the important differences in the results. Section 4 ends the paper with a summary and possible directions for future research, where we also present some results on the issue of gravitational corrections to the hydrogen atom spectrum in BST and JNW backgrounds. For the sake of completeness, we list, in two appendixes, the nonzero components of the Riemann curvature tensor in Fermi normal coordinates for circular geodesics in Schwarzschild and Bertrand space-times.

II. CIRCULAR GEODESICS AND FERMION CURVATURE COUPLINGS

We now consider an observer in circular geodesic motion and set up Fermi normal coordinates to compute fermion curvature couplings. We first set up the general formalism to be used in this section and later on in the paper. We begin with some statements which will set the notation and conventions, and will motivate the rest of the work.

A. Fermi normal coordinates and effective magnetic fields

In GR, in order to connect any result to possible experiments, we need a coordinate system in which the metric is locally flat along the entire geodesic on which our observer moves. As alluded to in the Introduction, such a system was envisaged in [14] by Manasse and Misner, and let us briefly recapitulate their construction, which involves a number of steps. First, we choose an arbitrary point on the geodesic G as the origin and set up a tetrad basis there. This basis is now parallely transported along the geodesic G and for any event at a point P with Fermi normal coordinates x^α, and the time x^0 is the proper time along G at the intersection of a spacelike hypersurface containing P, with G. The other components of P are obtained by proceeding along a spacelike geodesic on the hypersurface from the point of intersection. The tetrad basis (called the Fermi normal basis) should satisfy [14]

$$\hat{e}_\alpha.\hat{e}_\beta = \eta_{\alpha\beta}, \qquad \nabla_{\nu'}(\hat{e}^{\mu'}_\alpha)\hat{e}^{\nu'}_0 = 0, \tag{1}$$

where ∇ is the covariant derivative. Here, primes denote coordinates in which the original space-time metric is written (i.e., Schwarzschild or JNW or BST coordinates) and the unprimed indices will denote Fermi normal coordinates. Once we have set up the tetrad basis according to the above prescription, we can write down the components of the curvature tensor from those of the original space-time, using the explicit forms for the tetrads. These are given by

$$R_{\alpha\beta\gamma\delta} = \hat{e}^{\mu'}_\alpha \hat{e}^{\nu'}_\beta \hat{e}^{\rho'}_\gamma \hat{e}^{\sigma'}_\delta R_{\mu'\nu'\rho'\sigma'}. \tag{2}$$

Having obtained these, the metric around a geodesic G, to second order in the coordinates can be shown to be given by [14]

$$g_{00} = -1 + R_{0l0m}x^l x^m|_G, \qquad g_{0i} = \frac{2}{3}R_{0lim}|_G x^l x^m,$$
$$g_{ij} = \delta_{ij} + \frac{1}{3}R_{iljm}|_G x^l x^m, \tag{3}$$

where Latin indices are taken to be spatial, and it is to be noted that the curvature components are evaluated on G, where $x^i = 0$, i.e., on the geodesic, where the metric is that of flat space-time (with Lorentzian signature), $\eta_{\alpha\beta} = (-1, 1, 1, 1)$. Also note that the dependence on the observer's time enters the metric only through the components of the curvature that are evaluated at a given value of the proper time along the geodesic. Now having set up such a

coordinate system, we can analyze the covariant Dirac Lagrangian

$$\mathcal{L} = \sqrt{-g}(i\bar{\psi}\gamma^{\alpha}D_{\alpha}\psi - m\bar{\psi}\psi), \tag{4}$$

where γ^{α} are the usual Dirac matrices. First, a word about the notation is in order. We have three types of space-time metrics at play here: the original space-time that we start from, a locally flat metric at the fermion and finally a curved space-time around the geodesic given by the metric of Eq. (3). Following our previous notation, the primed coordinates will always refer to the original space-time. We will now use the beginning Greek indices $\alpha, \beta, \ldots$ to denote the locally flat metric. The later Greek indices like $\mu, \nu, \ldots$ will be used to denote the curved space-time surrounding our geodesic.

In Eq. (4), the covariant derivative and the spin connection have the standard definitions

$$D_{\alpha} = \left(\partial_{\alpha} - \frac{i}{4}\omega_{\beta\gamma\alpha}\sigma^{\beta\gamma}\right), \qquad \omega_{\alpha\beta\gamma} = e_{\alpha\mu}(\partial_{\gamma}e^{\mu}_{\beta} + \Gamma^{\mu}_{\nu\rho}e^{\nu}_{\beta}e^{\rho}_{\gamma}),$$
$$\sigma^{\alpha\beta} = \frac{i}{2}[\gamma^{\alpha}, \gamma^{\beta}], \tag{5}$$

where $\Gamma^{\mu}_{\nu\rho}$ is a Christoffel connection, and e^{μ}_{α} denotes a tetrad basis connecting the curved indices and flat indices near the geodesic. It can be shown [10,11] that the terms which come from the spin connection involve an interaction Lagrangian of the form $\bar{\psi}\gamma^{\alpha}\gamma^{5}b_{\alpha}$, where the four vector b can be written in a compact form,

$$b^{\sigma} = \epsilon^{\alpha\beta\gamma\sigma}e_{\beta\mu}(\partial_{\alpha}e^{\mu}_{\gamma} + \Gamma^{\mu}_{\nu\rho}e^{\nu}_{\gamma}e^{\rho}_{\alpha}) \equiv \epsilon^{\alpha\beta\gamma\sigma}e_{\beta\mu}\partial_{\alpha}e^{\mu}_{\gamma}, \tag{6}$$

where $\gamma^{5} = i\gamma^{0}\gamma^{1}\gamma^{2}\gamma^{3}$, and it can be checked that b_0 is identically zero. Importantly, in a Hamiltonian approach, this interaction Lagrangian can be cast into an effective interaction energy of the form $-\vec{b}.\vec{s}$ in the nonrelativistic limit, as shown in [12] (see also [8]). This involves starting from a relativistic Dirac Lagrangian and extracting a nonrelativistic quantum Hamiltonian by following a sequence of Foldy-Wouthuysen transformations with appropriate field redefinitions. The fact that the interaction Lagrangian of Eq. (6) can be cast into this nonrelativistic form is the basis of gravitation induced apparent *CPT* violation in the EOT-Wash experiment. In our case, as explained in [10], the effective magnetic fields[1] $\vec{b}$ will change sign under parity, and hence gravitational curvature couplings will not (apparently) violate *CPT*. These magnetic fields might, however, form the basis of other detectable gravitational effects.

We should clarify here that in many of the examples that we deal with in this paper, our results are for relativistic orbits. This is the orbit that our observer travels in, but we assume that the experiment is performed on nonrelativistic fermions, in the observer's coordinate basis. So it makes sense to talk about fermion interactions in the nonrelativistic limit of the Dirac equation. It might be interesting to generalize our results beyond the nonrelativistic limit, by incorporating corrections in the approach of [12]. However, this might be a difficult exercise, and we will not pursue this topic for the purpose of the present work.

To compute the magnetic fields, we will need the tetrads [5,7]

$$e^{\mu}_{0} = \delta^{\mu}_{0} - \frac{1}{2}R^{\mu}{}_{\alpha 0\beta}|_{G}x^{\alpha}x^{\beta}, \qquad e^{\mu}_{i} = \delta^{\mu}_{i} - \frac{1}{6}R^{\mu}{}_{jik}|_{G}x^{j}x^{k}, \tag{7}$$

where i, j and k run over the spatial indices only. Hence, to calculate the b_i's which is one of our main interests in this paper, we require setting up the tetrad basis of Eq. (1) to evaluate the components of the Riemann tensor in Fermi normal coordinates. We then use this input in Eq. (6) along with the tetrads in Eq. (7) to obtain the fields. The effect of gravity will enter the field through the curvature tensor. As we have mentioned, b_0 vanishes identically, and the expression for the spatial components $\vec{b}$ are given by [10]

$$b_{i} = \frac{1}{4}\epsilon_{0\gamma\beta i}R^{\gamma\beta}{}_{0l}|_{G}x^{l} + \frac{1}{4}\epsilon_{0\gamma\beta i}R^{0\beta\gamma}{}_{l}|_{G}x^{l}. \tag{8}$$

Hence, knowing $R_{\alpha\beta\gamma\delta}$, we can compute the effective magnetic field in the nonrelativistic limit due to gravitational interactions, and in cases of interest, this should be contrasted with the intrinsic magnetic fields present in some celestial objects.

One has to be careful with the coordinates of the event here, since the metric in Fermi normal coordinates of Eq. (3) is valid only close to the geodesic. If the measurement is carried out on the geodesic where $x^{l} = 0$, $\vec{b}$ vanishes identically. Typically, in computations related to the hydrogen atom (which is in free fall) for example, the hypothetical observer is located at the nucleus of the atom, and the x^{i}s are hence of the order of the Bohr radius [5]. For the purpose of our discussion, we will keep the observer's coordinate explicit, and in some cases where we discuss quantitative results, we will take this to be of order unity,

[1]Throughout this work we deal with effective magnetic fields, or gravitomagnetic fields that are not actual magnetic fields in the sense that they do not arise due to movement of charges. To avoid repetition of terminology, we will sometimes loosely call these magnetic fields, although we make it clear to the reader that we will only deal with effective magnetic fields due to gravitational effects.

since we are mainly interested in experiments involving finite size apparatus.

A few words about the magnitudes of $\vec{b}$ is also in order. Present day bounds on the effective magnetic fields can be obtained from the fact that$\vec{b}$ translates to a magnetic field $\vec{B} = \vec{b}/\mu_B$ where μ is the Bohr magneton. Using $\mu_B = 9.3 \times 10^{-24}$ J/T, the fact that $\vec{B}$ can be measured up to an accuracy of 10^{-12} Gauss translates into $|\vec{b}| \sim 10^{-28}$–10^{-29} GeV [8,17]. Hence, if we consider a realistic situation and $\vec{b}$ turns out to be of this order, then we can hope to detect it. However, as we point out in the sequel, the values of the magnetic fields that we obtain are much less than present day bounds, and hence we can only hope that these will be detected in futuristic experiments. However, we do not rule out the fact that indirect evidence of strong magnetic fields due to gravitational effects might be possible to observe.

Before we begin our analysis, let us point out what we expect. On physical grounds, we expect that large $\vec{b}$ should occur in regions where gravitational effects are large and our observer is close to an instability. For circular geodesics, vacuum solutions of Einstein's equations dictate that such instabilities can occur near a photon sphere [18] which is defined as a timelike hypersurface, such that a null geodesic that is tangent to this hypersurface at some point of time will remain so in the future. For the Schwarzschild black hole, the photon sphere is at $r = \frac{3}{2}R_s$, with R_s being the Schwarzschild radius, and at this value of the radial coordinate, the energy and angular momentum per unit mass of a test particle undergoing circular geodesic motion becomes very large; i.e., the motion is highly relativistic. Indeed, it is well known that the scalar-field power spectrum from particles in circular geodesics in a Schwarzschild background sharply peaks near the photon sphere [19]. We expect that $\vec{b}$ should be large in this limit for Schwarzschild and for similar limits in the JNW space-times as well, where behavior of circular geodesics is qualitatively similar to (but has a richer structure than) Schwarzschild backgrounds. Here, we run into an important issue of stability of orbits. Circular orbits near the photon sphere in exterior Schwarzschild backgrounds are unstable, and hence the physics of magnetic fields for such orbits is somewhat unclear. However, as we will show, there are stable orbits for which the fields will be large, and in these cases the physicality of our results is guaranteed. Also, for BSTs that we consider later, there is no photon sphere. Here, stable circular orbits are possible close to the central singularity, by construction. In this case, we expect that the magnetic field becomes large only close to the singularity. We will indeed see that these expectations are met.

For radial geodesics, the situation is different. Here, in general we would expect the field $\vec{b}$ to depend on the energy of the observer, since generically this would appear in the curvature (an important exception being the Schwarzschild solution). Hence, in this case, the results will depend on the observer's velocity. More energetic observers should feel the effect of gravity more than less energetic ones, and this is what we also find from our results.

B. Fermi normal coordinates for circular geodesics in static, spherically symmetric space-times

We consider a general static, spherically symmetric space-time with metric[2]

$$ds^2 = -c^2A(r)dt^2 + B(r)dr^2 + G(r)d\Omega^2, \tag{9}$$

where $A(r)$, $B(r)$ and $G(r)$ may be arbitrary positive functions of the radial coordinate, and $d\Omega^2 = d\theta^2 + \sin^2\theta d\phi^2$ is the standard metric on the unit two sphere. The form of the metric dictates that we have the conserved quantities

$$\epsilon = c^2A(r)\dot{t}, \qquad L = G(r)\dot{\phi}, \tag{10}$$

which are the energy per unit mass and angular momentum per unit mass of the test particle, respectively. Here and in what follows, the dots denote derivatives with respect to the proper time on the geodesic and the primes will denote a derivative with respect to r. For timelike geodesics, we have

$$\dot{r}^2 + V(r) = 0, \qquad V(r) = \frac{1}{B(r)}\left[-\frac{\epsilon^2}{c^2A(r)} + \frac{L^2}{G(r)} + c^2\right]. \tag{11}$$

For circular orbits, using $V(r) = V'(r) = 0$, we obtain

$$\epsilon = \frac{c^2A(r)\sqrt{G'(r)}}{\sqrt{G'(r)A(r) - G(r)A'(r)}}, \qquad L = \frac{cG(r)\sqrt{A'(r)}}{\sqrt{A(r)G'(r) - G(r)A'(r)}}. \tag{12}$$

Now one can set up the Fermi normal tetrad basis as follows (the Schwarzschild case was worked out in [7]):

[2]We will keep the factors of the speed of light c explicit for the moment, so that dimensional consistency of our results can be verified at each stage. For qualitative discussions, we will set $c = 1$.

$$\hat{e}_0^{\mu'} = \left(\frac{\epsilon}{c^3 A(r)}, 0, 0, \frac{L}{cG(r)}\right), \quad \hat{e}_1^{\mu'} = \left(-\frac{L\sin(\phi(\tau)\delta(r))}{c^2\sqrt{A(r)G(r)}}, 0, \frac{\cos(\phi(\tau)\delta(r))}{\sqrt{B(r)}}, 0, -\frac{\epsilon\sin(\phi(\tau)\delta(r))}{c^2\sqrt{A(r)G(r)}}\right),$$
$$\hat{e}_2^{\mu'} = \left(0, 0, \frac{1}{\sqrt{G(r)}}, 0\right), \quad \hat{e}_3^{\mu'} = \left(\frac{L\cos(\phi(\tau)\delta(r))}{c^2\sqrt{A(r)G(r)}}, \frac{\sin(\phi(\tau)\delta(r))}{\sqrt{B(r)}}, 0, \frac{\epsilon\cos(\phi(\tau)\delta(r))}{c^2\sqrt{A(r)G(r)}}\right), \tag{13}$$

where we have defined

$$\delta(r) = \frac{1}{2}\sqrt{\frac{G'(r)(A(r)G'(r) - G(r)A'(r))}{A(r)B(r)G(r)}}. \tag{14}$$

For example, for the Schwarzschild black hole, this factor is $\delta(r) = \sqrt{1 - \frac{3R_s}{2r}}$, where $R_s = \frac{2GM}{c^2}$ is the Schwarzschild radius and G denotes Newton's constant.

It can be checked that the form of the tetrad above satisfies the conditions in Eq. (1). Now we can compute the components of the curvature tensor in the coordinates of Eq. (9) and use Eqs. (2) and (13) to obtain the curvature components in Fermi normal coordinates. The calculations are lengthy, but can easily be performed using a standard MATHEMATICA routine. The expressions are large, and we omit them for brevity. We use Eq. (8) to evaluate the effective magnetic field due to curvature couplings and find that

$$\begin{aligned}
b_0 &= 0,\\
b_1 &= \frac{\sqrt{A'G'}[GA'G' + A(4BG - G'^2)]}{16BA^{1/2}G^{3/2}(AG' - GA')} y\cos(\phi(\tau)\delta),\\
b_2 &= \frac{P(r)}{Q(r)},\\
b_3 &= \frac{\sqrt{A'G'}[GA'G' + A(4BG - G'^2)]}{16BA^{1/2}G^{3/2}(AG' - GA')} y\sin(\phi(\tau)\delta),
\end{aligned} \tag{15}$$

where $P(r)$ and $Q(r)$ are defined as

$$\begin{aligned}
P(r) &= \sqrt{A'G'}[B(2A^2GG'' - A^2G'^2 + G^2(A'^2 - 2AA'')) \\
&\quad + AGB'(GA' - AG')](x\cos(\phi(\tau)\delta) + z\sin(\phi(\tau)\delta)),\\
Q(r) &= 16B^2(AG)^{3/2}(AG' - GA'),
\end{aligned} \tag{16}$$

and x, y, z are the observer's spatial coordinates. If $x^i = 0$, i.e., the measurements are carried out on the geodesic, the magnetic field is zero as expected, as Fermi normal coordinates are flat there. In what follows, we will present our results by setting $x^i \sim O(1)$. In graphical analysis, we will calculate the fields in units of the observer's typical length, which we denote by R_o. In spherical polar coordinates, this will be the radius of the event.

Equation (15) is the master equation for this section, and it can be used to compute the effective magnetic field for any static, spherically symmetric metric. Having outlined the general calculation scheme, we will now specialize to our cases of interest. The first case we consider is fermions in circular motion in the background of the Schwarzschild solution.

C. Circular geodesics in exterior and interior Schwarzschild space-times

We start with the familiar exterior Schwarzschild metric

$$ds^2 = -\left(1 - \frac{R_s}{r}\right)c^2dt^2 + \left(1 - \frac{R_s}{r}\right)^{-1}dr^2 + r^2d\Omega^2. \tag{17}$$

The energy and angular momentum per unit mass of a particle in circular geodesic is given in the Schwarzschild background as

$$\epsilon = \frac{c^2(1 - \frac{R_s}{r})}{\sqrt{1 - \frac{3R_s}{2r}}}, \qquad L = \sqrt{\frac{c^2r^2R_s}{2r - 3R_s}}. \tag{18}$$

In this case, our calculation yields, from the master Eq. (15),[3]

$$\begin{aligned}
b_1 &= \mathcal{A}y\cos(\phi(\tau)\delta),\\
b_2 &= \mathcal{A}(x\cos(\phi(\tau)\delta) + z\sin(\phi(\tau)\delta)),\\
b_3 &= \mathcal{A}y\sin(\phi(\tau)\delta),
\end{aligned} \tag{19}$$

where we have defined

$$\mathcal{A} = \frac{3\sqrt{R_s^3(r - R_s)}}{4\sqrt{2}r^3(2r - 3R_s)}. \tag{20}$$

Let us analyze this result in some detail.[4] First, we note from Eq. (19) that the magnetic field blows up close to $r = \frac{3}{2}R_s$, the location of the photon sphere (below this radius, circular orbits do not exist). As alluded to earlier in

[3]We list in Appendix A the nonzero components of the Riemann tensor for circular geodesics in Schwarzschild backgrounds, also obtained in [20].

[4]For ease of notation, we will henceforth write the magnetic fields in units of the observer's coordinates, ignoring the angular factor. This will not lead to any loss of generality of our results, while avoiding cluttering notations. Thus, we will calculate b_i/R_o, where R_o is a typical coordinate of the observer defined at the end of Sec. II B. However, we will keep denoting this as b_i. The full expression for the fields will typically look like that in Eq. (19).

this section, although the circular orbit is unstable at this radius, this implies that a gravitational contribution to the magnetic field can be very large here. To get a physically meaningful situation, we should have an object whose radius is of the order of its Schwarzschild radius. A neutron star is a candidate which fits this requirement, and hence our result is indicative of the fact that near the photon sphere of a neutron star, GR effects can generate a very large magnetic field on a fermion in circular motion. Of course, as said in the Introduction, this is to be distinguished from the intrinsic magnetic fields of such objects whose physics is very different. The field falls off as $\sim r^{-\frac{7}{2}}$ as a function of the radial distance, for large r. In Fig. 1, we plot the magnetic field as a function of the distance, with $R_s = 1$. As a numerical estimate, upon restoring factors of $\hbar$ and setting $R_s = 10^3 m$ (a typical Schwarzschild radius for a neutron star) we obtain $|\vec{b}| \sim 10^{-24}$ GeV at a distance $r = 3R_s$, where stable orbits exist. We also note that in the direction of the magnetic field, given say in the x-z plane of the observer by $\tan^{-1}(\frac{b_3}{b_1})$, the r dependence enters only via $\delta(r)$. Far from the black hole, this quantity is small, and hence in this regime, the direction of the magnetic field will be independent of the Schwarzschild radial coordinate r.

In is instructive to contrast the results above with those obtained from an interior Schwarzschild solution. To simplify notations, we will define

$$\alpha = \frac{3}{2}\sqrt{1-\frac{R_s}{R}}, \qquad \kappa = \frac{R_s}{R^3}, \qquad X = \left(\alpha - \frac{1}{2}\sqrt{1-\kappa r^2}\right)^2. \tag{21}$$

Then the well known interior Schwarzschild solution, describing a fluid of constant density, is given by

$$ds^2 = -c^2 X dt^2 + \frac{dr^2}{1-\kappa r^2} + r^2 d\Omega^2, \tag{22}$$

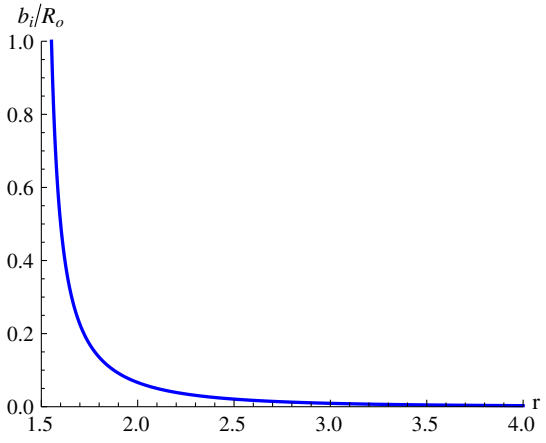

FIG. 1 (color online). Effective magnetic field in units of the observer's length scale, as a function of distance for the exterior Schwarzschild solution, with $R_s = 1$.

the solution being valid for $r \leq R$, R being the matching radius where the interior solution goes over to an external Schwarzschild one. Here, we will use the conserved energy and angular momentum per unit mass, given as

$$\epsilon = c^2\sqrt{\frac{\sqrt{1-\kappa r^2}\left(\sqrt{1-\kappa r^2}-2\alpha\right)^3}{4\left(1-2\alpha\sqrt{1-\kappa r^2}\right)}},$$
$$L = cr^2\sqrt{\frac{\kappa}{2\alpha\sqrt{1-\kappa r^2}-1}}, \tag{23}$$

respectively. In this case, general results for the magnetic field derived from our master Eq. (15) is lengthy and not very illuminating. We find that for small values of r, the fields start from small values, and their magnitudes increase as r increases. This is expected, as our observer experiences more gravitating mass as the radial distance increases, and hence the effective magnetic field also increases. Thus, the magnetic field will be strongest at the matching radius. At this value $r = R$, the expressions for the fields simplify, and we get

$$b_1 = b_3 = -b_2 = \frac{3\sqrt{R_s^3(R-R_s)}}{4\sqrt{2}R^3(2R-3R_s)}. \tag{24}$$

Note the similarity of this expression with the results obtained from the exterior Schwarzschild solution [Eqs. (19) and (20)]. The solutions match but for a negative sign in b_2. Of course, this is insignificant, since the fields depend on the derivatives of the metric, and these need not be continuous at the matching radius. We see, however, that in this case also, a large magnetic field might be generated in the interior region, if $(r =)\ R = \frac{3}{2}R_s$, but importantly, circular orbits are stable here. That is, at $r = R$, the conserved energy and angular momentum per unit mass blows up; i.e., the circular orbit is highly relativistic but is stable as can be checked by calculating the effective potential. Typically, such a situation might again be of relevance in the context of highly gravitating objects like black holes or neutron stars. In Fig. 2, we show this result graphically. Here we have set $R_s = 1$ and $R = 1.5$. Note that in the context of the interior Schwarzschild solution, R has to satisfy the Buchdahl bound, i.e., $R > 9/8$, so that the pressure of the interior fluid is finite.

D. Circular geodesics in JNW space-times

Next, we move on to consider circular geodesics in the Janis-Newman-Winicour space-times. These are space-times sourced by a scalar field; i.e., this is an Einstein-Klein-Gordon system, given by the metric

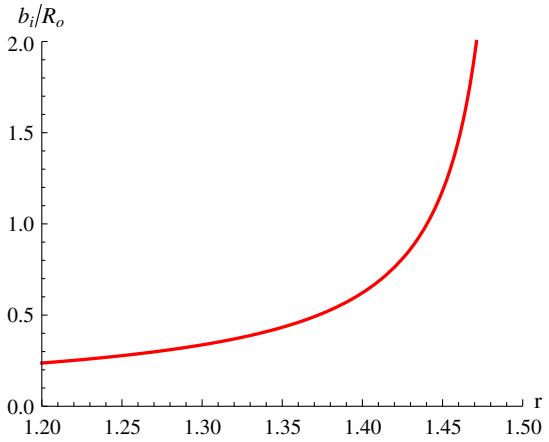

FIG. 2 (color online). Effective magnetic field in units of the observer's length scale, for the interior Schwarzschild solution, with $R_s = 1$, $R = 1.5$.

$$ds^2_{\rm JNW} = -c^2\left(1-\frac{B}{r}\right)^{\nu} dt^2 + \frac{1}{(1-\frac{B}{r})^{\nu}} dr^2 + r^2\left(1-\frac{B}{r}\right)^{1-\nu} d\Omega^2. \tag{25}$$

Here, ν is a parameter that ranges from 0 to 1. As is well known, the singularity of this space-time at $r = B$ is globally naked. Also, the source of the JNW space-time is a scalar field,

$$\psi = \frac{q}{B\sqrt{4\pi}} \ln\left(1-\frac{B}{r}\right), \tag{26}$$

where q is a parameter that denotes its magnitude. The ADM mass M is related to B and q by $B = 2\sqrt{q^2+M^2}$, and also $\nu = 2M/B$.[5] Setting $\nu = 1$, i.e., $q = 0$, one recovers the Schwarzschild metric. For JNW space-times, we use the conserved energy and angular momentum per unit mass as

$$\epsilon = c^2\sqrt{\left(1-\frac{B}{r}\right)^{\nu}\left(1+\frac{B\nu}{2r-2B\nu-B}\right)}, \qquad L = cr\sqrt{\frac{B\nu(1-\frac{B}{r})^{1-\nu}}{2r-2B\nu-B}}. \tag{27}$$

Now we can calculate the magnetic fields as before. For illustration, we will set $B = 1$, in which case the fields take a simple form

$$b_1 = b_2 = b_3 = \frac{(r-1)^{\nu-2} r^{-\nu-2}(\nu(6r-3)-2\nu^2-1)\sqrt{\nu(2r-\nu-1)}}{16(2r-2\nu-1)}. \tag{28}$$

For $\nu \to 1$, this goes over to the Schwarzschild result, as expected. To analyze Eq. (28), we first note that the photon sphere for the JNW singularity is at

$$r_{\rm ps} = \frac{B}{2}(1+2\nu). \tag{29}$$

This is the radius at which the energy and angular momentum per unit mass of Eq. (27) diverges. It is also known from an analysis of the stability of circular orbits that three distinct regions in ν need to be considered. Defining

$$r_{\pm} = \frac{B}{2}\left(1+3\nu \pm \sqrt{5\nu^2-1}\right), \tag{30}$$

the ranges of stable orbits corresponding to different values of ν are (see, e.g., [21])

$$\begin{aligned} &\text{Case 1}: 0 < \nu < \frac{1}{\sqrt{5}}, \quad B < r < \infty; \\ &\text{Case 2}: \frac{1}{\sqrt{5}} < \nu < \frac{1}{2}, \quad B < r < r_- \quad \text{and} \quad r_+ < r < \infty; \\ &\text{Case 3}: \frac{1}{2} < \nu < 1, \quad r_+ < r < \infty. \end{aligned} \tag{31}$$

Now from Eq. (28), we see that the magnetic field becomes very large near the photon sphere, whenever it exists. Specifically, from this equation, b_i diverges at $r = r_{\rm ps} = \frac{1}{2}(1+2\nu)$ and at $r = B = 1$. Let us first consider case I. As a representative value, we choose $\nu = 0.43$. Here, stable orbits exist at all radii. In Fig. 3, we have shown this case with the solid blue line, where the field is plotted as a function of the radial distance r. They diverge close to the singularity at $r = 1$. Next, we consider case 2, where we have chosen $\nu = 0.49$. Stable orbits exist for $r < 1.01$ and for $r > 1.46$. The dashed red curve of Fig. 3 depicts the fields in this case. We see that there is a divergence in the fields at $r = 1$. There is a maximum of the field at $r = 1.007$, where in units of the observer's coordinates, $b_i \sim 17$ (in appropriate energy units). At both these values of r, the orbits are stable. For case 3, we find that the fields become large only near the photon sphere, where circular orbits are highly relativistic, but unstable. In Fig. 4, we show this situation for $\nu = 0.7$ (solid blue curve) and for $\nu = 0.8$ (dashed red curve). The radii of the photon sphere are at $r = 1.2$ and $r = 1.3$, respectively.

[5]We will set $G = c = 1$ here. Setting $B = 1$ fixes $M = \frac{\nu}{2}$ for a given value of ν. This sets the value of q via $q^2 = \frac{1}{4} - M^2$.

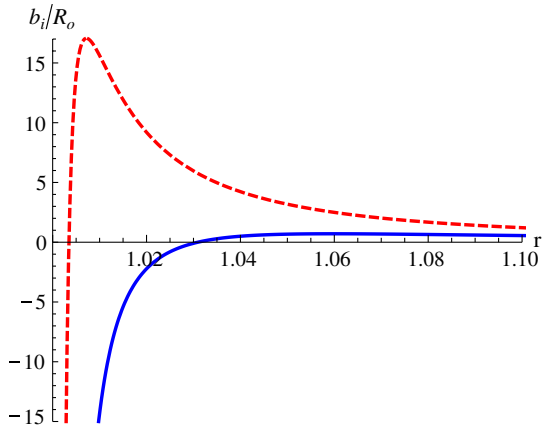

FIG. 3 (color online). Effective magnetic fields as a function of the radial distance for JNW space-time with $\nu = 0.43$ (solid blue line) and $\nu = 0.49$ (dashed red line).

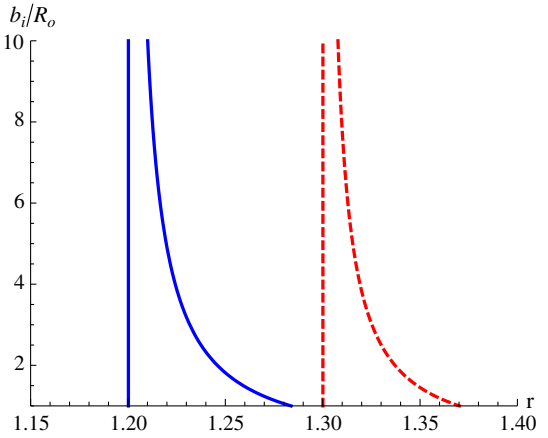

FIG. 4 (color online). Effective magnetic fields as a function of the radial distance for JNW space-time with $\nu = 0.7$ (solid blue lines) and $\nu = 0.8$ (dashed red lines).

E. Circular geodesics in Bertrand space-times

We will now consider circular geodesics in BSTs. First let us recall a few definitions. BSTs were discovered by Perlick [22], as solutions of Einstein gravity where each spatial point admits a closed stable orbit. This generalizes the well known Bertrand's theorem [23] to GR. That such space-times can be good candidates for galactic dark matter was pointed out in [15] from the assumption that stars away from Galactic centers follow approximately circular orbits. The metric for a BST (of type II, in the classification of [22]) is given by

$$ds^2_{\rm BST} = -\frac{c^2dt^2}{D+\frac{\alpha}{r}} + \frac{dr^2}{\beta^2} + r^2d\Omega^2. \tag{32}$$

Here, α and D are positive, β is a rational number, and $r_s = \frac{\alpha}{D}$ is related to the galactic length scale, in the sense that if we take r_s to be of the size of the galaxy, then in the Newtonian limit, reasonable estimates to the mass of the galaxy can be obtained. Indeed, a phenomenological definition of the circular velocity of matter (considered as a perturbation over the BST background such that backreaction effects are neglected) gives results that match well with experimental data on low surface brightness galaxies. In a Newtonian approximation, these also reproduce the popular Navarro-Frenk-White (NFW) [24] and Hernquist [25] density profiles for the dark matter distribution, in appropriate limits [15]. We will consider this model in a phenomenological spirit and estimate effective magnetic fields for observers in geodesic motion in this matter distribution, even close to the Galactic center. Note that there is a central singularity at $r = 0$ in the metric of Eq. (32) which is naked.

Here, we evaluate $\vec{b}$ by setting $\beta = 4/5$.[6]

$$b_1 = \frac{\alpha(17\alpha+9Dr)}{50\sqrt{2}r^2\sqrt{\alpha(\alpha+Dr)}(\alpha+2Dr)} = b_3,$$
$$b_2 = \frac{\sqrt{2}(\frac{\alpha}{\alpha+Dr})^{3/2}(\alpha+4Dr)}{25r^2(\alpha+2Dr)}. \tag{33}$$

First of all, we note from the above expressions that for small distances $Dr \ll \alpha$, $b_i \sim r^{-2}$. For large distances, we have b_1 and $b_3 \sim r^{-\frac{5}{2}}$ while $b_2 \sim r^{-\frac{7}{2}}$. Specifically, in the first case, we see that b_i becomes independent of α and D, and $\sim r^{-2}$, whereas in the opposite limit, we obtain b_1, $b_3 = K_1 r_s^{\frac{1}{2}} r^{-\frac{5}{2}}$ and $b_2 = K_2 r_s^{\frac{3}{2}} r^{-\frac{7}{2}}$, where K_1 and K_2 are numerical constants. The fact that the fields blow up as $r \to 0$ is expected, since the energy density in BSTs also blows up in this limit [15]. Also, we see that the direction of the magnetic field in one of the planes of the observer (the X-Y plane in this case) is dependent on r,

$$\frac{b_2}{b_1} = \frac{4\alpha(\alpha+4Dr)}{(\alpha+Dr)(17\alpha+9Dr)}, \tag{34}$$

a result that is qualitatively different from a Schwarzschild background.

Now, we note that from a Newtonian perspective, a fit of the circular velocities of galactic rotation curves relates the parameters α and D to the maximum value of the circular velocity and the Newtonian mass of the galaxy as [Eqs. (8) and (12) of [15]]

$$\alpha = \frac{c^2GM}{8(v_c^{\rm max})^4}, \qquad D = \frac{c^2}{8(v_c^{\rm max})^2}, \tag{35}$$

[6]Nonzero components of the Riemann tensor for circular geodesics in BSTs are listed in Appendix B.

where $\frac{\alpha}{D}$ can be taken to be an estimate of the size of the galaxy. If we input these values in the expressions for the magnetic field of Eq. (33), we obtain

$$b_1 = b_3 = \frac{17GM + 9r(v_c^{\max})^2}{50r^2(GM + 2r(v_c^{\max})^2)\sqrt{2 + \frac{2r(v_c^{\max})^2}{GM}}},$$
$$b_2 = \frac{\sqrt{2}\left(\frac{GM}{GM + r(v_c^{\max})^2}\right)^{3/2}(GM + 4r(v_c^{\max})^2)}{25r^2(GM + 2r(v_c^{\max})^2)}. \quad (36)$$

Now we can take a typical estimate of $M \sim 10^8 M_\odot$ and $v_c^{\max} = 30$ km/s (which describe the galaxy NGC4395 to a good approximation), to obtain $b_i \sim 10^{-26}$ GeV for $r \sim 10^4$ m.[7] This is, of course, a somewhat unrealistic estimate, since we have taken r to be very small compared to the galactic scales, but might be observationally important. If we take $r = \alpha/D$, which is an estimate for the galactic size, we obtain

$$b_i \sim \frac{(v_c^{\max})^4}{G^2M^2}, \quad (37)$$

and taking the typical values of M and $v_c^{\max}$ indicated above, we obtain $b_i \sim 10^{-55}$ GeV which is too small to detect in present experiments.

III. RADIAL GEODESICS AND FERMION CURVATURE COUPLINGS

We now turn to observers in radial geodesics as described by Fermi normal coordinates. We will first demonstrate the general construction of Fermi normal coordinates for radial motion in static, spherically symmetric space-times, and present the results for the effective magnetic field in the general case. Then we will specialize to some examples.

A. Fermi normal coordinates for radial geodesics in static, spherically symmetric space-times

We start with the general metric of Eq. (9). For radial geodesics, we set up the tetrad

$$\hat{e}_0^{\mu'} = \left(\frac{\dot{t}}{c}, \frac{\dot{r}}{c}, 0, 0\right), \qquad \hat{e}_1^{\mu'} = \left(\frac{\dot{r}}{c^2}\sqrt{\frac{B(r)}{A(r)}}, \dot{t}\sqrt{\frac{A(r)}{B(r)}}, 0, 0\right),$$
$$\hat{e}_2^{\mu'} = \left(0, 0, \frac{1}{\sqrt{G(r)}}, 0\right), \qquad \hat{e}_3^{\mu'} = \left(0, 0, 0, \frac{1}{\sqrt{G(r)}\sin\theta}\right), \quad (38)$$

where the dot denotes a derivative with respect to the proper time along the radial geodesic. Now one can check that the conditions of Eq. (1) are satisfied, upon using the radial geodesic equation in this background. We also use the normalization condition for radial geodesics,

$$\dot{t} = \sqrt{\frac{c^2 + B(r)\dot{r}^2}{c^2A(r)}} = \frac{\epsilon}{c^2A(r)}, \quad (39)$$

where ϵ is the conserved energy per unit mass of our test particle, as before. Now we can compute the effective magnetic field. We find that $b_0 = b_1 = 0$, and

$$b_2 = z\mathcal{B}, \qquad -b_3 = y\mathcal{B},$$
$$\mathcal{B} = \frac{1}{16cBG^2}z\dot{r}\sqrt{\frac{B(r)\dot{r}^2 + c^2}{A(r)c^2}}(M(r) + N(r)). \quad (40)$$

where we have defined

$$M(r) = \sqrt{\frac{A}{B}}BG'^2,$$
$$N(r) = G\left(\sqrt{\frac{B}{A}}A'G' + \sqrt{\frac{A}{B}}(B'G' - 2BG'')\right). \quad (41)$$

Equation (40) is the master equation for this section, and we will now proceed to analyze special cases of this result.

B. Radial geodesics in Schwarzschild, JNW and Bertrand space-times

For the exterior vacuum Schwarzschild solution, we set up the Fermi normal coordinates as prescribed in [14] [or from Eq. (38)]. Here, we find that all components of the effective magnetic field are identically zero. Interestingly, the situation changes for interior Schwarzschild solutions, described by Eqs. (21) and (22). Here, we find that the magnetic field at the interior is nonzero, and it does not fall off to zero at the matching radius, as one would have naively expected. In fact, at the matching radius $r = R$, we find that

$$b_2 = \frac{3R_s\epsilon}{8c^4R^2(R - R_s)}\sqrt{\epsilon^2 - c^4\left(1 - \frac{R_s}{R}\right)}. \quad (42)$$

This can be large for R close to R_s and for large values of ϵ. Hence, there is a discontinuity for $\vec{b}$ at the matching radius. This is not surprising, since, as mentioned before, the fields depend on the derivatives of the metric, which can be discontinuous at the matching radius. In Fig. 5, we show the behavior of the field b_2 (in units of the observer's coordinates) as a function of the radial coordinate, for $\epsilon = 5$ and 6 (in units of c^2). The same qualitative feature is seen for a fermion in radial geodesic motion in a JNW background of Eq. (25). Here, we find that

[7] Upon restoring all units, the b_i's are of dimension L^{-1}. This has to be multiplied by $\hbar c$ in order to get the field in GeV.

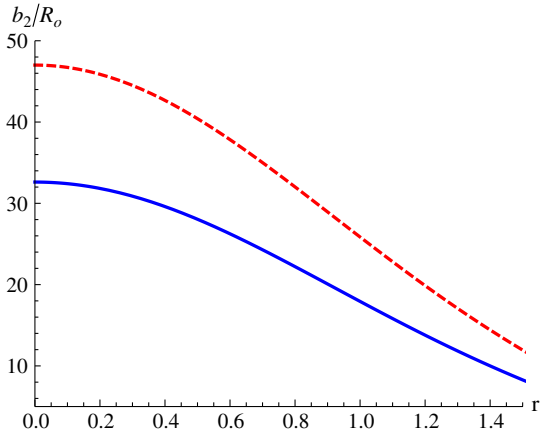

FIG. 5 (color online). Effective magnetic fields as a function of the radial distance for the interior Schwarzschild space-time with $\epsilon = 5c^2$ (solid blue line) and $\epsilon = 6c^2$ (dashed red line).

$$b_3 = -b_2 = \frac{\epsilon B^2(\nu^2-1)\sqrt{\epsilon^2 - c^4(1-\frac{B}{r})^{\nu}}}{16c^4 r^2 (B-r)^2}. \quad (43)$$

Recalling that for radial geodesics in the JNW geometry, we have

$$\dot{t} = \frac{\epsilon}{c^2}\left(1-\frac{B}{r}\right)^{-\nu}, \qquad \dot{r} = \left[\frac{\epsilon^2}{c^2} - c^2\left(1-\frac{B}{r}\right)^{\nu}\right]^{\frac{1}{2}}, \quad (44)$$

we see that the field vanishes for $\dot{r} = 0$ and in general can be large for large values of ϵ and small values of r.

Finally, we repeat the analysis for radial geodesics in BST backgrounds. First, let us recapitulate a few details [15]. For radial geodesics, it can be checked that

$$\dot{t} = \frac{\epsilon}{c^2}\left(D + \frac{\alpha}{r}\right), \qquad \dot{r} = \beta\left[\frac{\epsilon^2}{c^2}\left(D+\frac{\alpha}{r}\right) - c^2\right]^{\frac{1}{2}}. \quad (45)$$

Hence, the radial velocity is given by

$$v_{\rm rad} = \frac{\beta c\sqrt{r}}{\varepsilon(\alpha + Dr)}[\epsilon^2(Dr+\alpha) - c^4 r]^{\frac{1}{2}}. \quad (46)$$

From Eq. (46) we see that the radial velocity thus becomes zero if the energy per unit mass satisfies

$$\epsilon^2 = \frac{c^4 r}{\alpha + Dr}, \quad (47)$$

which can also be turned around to provide a maximum value of the radius at which the particle reaches zero velocity. Now, after transforming to Fermi normal coordinates, we calculate the components of the effective magnetic field and find that (with $b_0 = b_1 = 0$),

$$b_2 = -b_3 = \frac{2\alpha\epsilon}{25c^4 r^3}\sqrt{\frac{\epsilon^2(\alpha+Dr) - c^4 r}{\alpha + Dr}}, \quad (48)$$

where we have set the parameter $\beta = 4/5$. Hence, the field is dependent on the energy of the observer and is zero for the value of ϵ given in Eq. (47). Now if we use Eq. (35) to obtain the field in a galactic scenario, we obtain

$$b_2 = \frac{GM\epsilon}{100c^2(v_c^{\rm max})^4 r^3}\sqrt{\frac{\epsilon^2(GM + (v_c^{\rm max})^2 r) - 8c^2(v_c^{\rm max})^4 r}{GM + (v_c^{\rm max})^2 r}}. \quad (49)$$

For a highly relativistic particle, this can be large. For example, if we take $M = 10^8 M_{\odot}$, with $v_c^{\rm max} = 20$ Km/s and set $\epsilon = 10^{16}$ $(\rm m/s)^2$, then we obtain, at a radius of $\sim 10^6$ m, $b_2 \sim 10^{-11}$ GeV. This can be significant in futuristic experiments.

IV. DISCUSSIONS AND CONCLUSIONS

In this paper, we have considered the effective magnetic field due to curvature couplings in fermions. These arise purely due to gravity effects and are different in origin from intrinsic magnetic fields. Using Fermi normal coordinates, we have computed these for the Schwarzschild, JNW and Bertrand space-times, for observers in circular and radial geodesics. Our results establish the qualitative difference in the fields in various cases. We show that these fields can be large for specific parameter values in the theories, and hence might be indirectly observed in futuristic experiments.

For circular geodesics, whereas the direction of the effective magnetic field remains a constant as a function of the radial coordinate for the Schwarzschild and JNW backgrounds, this is not true for naked singularity backgrounds seeded by galactic dark matter. It was also shown that for Schwarzschild and JNW backgrounds, there is a large enhancement of the effective magnetic field not only near the photon sphere but also in regimes where circular orbits are stable. As we have mentioned, this might have implications for highly gravitating objects like black holes or neutron stars. However, such enhancement is not observed in BST backgrounds. For the latter, large fields are seen by circular observers only close to the singularity.

For observers on radial geodesics, our results show that whereas an external Schwarzschild observer will not see any effective magnetic field, the same is not true for internal Schwarzschild, JNW, and BST observers. This is an important distinction between vacuum space-times and those seeded by matter, and should be investigated further. In these cases, the field is dependent on the observer's energy and can be considerably large for highly relativistic observers.

Before we conclude, we mention that our results for the JNW and the BST can be used to make a comparative analysis of gravitational effects on the hydrogen atom

spectra, which has been well studied in the literature [5,6] by using degenerate perturbation theory. We will consider only nonrelativistic energy shifts and will simply state our main results here. For the $1S$ and $2S$ states of the hydrogen atom, in Schwarzschild backgrounds, the nonrelativistic energy shifts are zero [Eqs. (6.1) and (6.15) of [7]]. The essential reason is that these are proportional to the R_{00} component of the Ricci tensor, which is identically zero for radial and circular geodesics in the Schwarzschild geometry, in Fermi normal coordinates. For JNW and BST backgrounds, this ceases to be the case (see Appendix B for the explicit expression of R_{00} for circular geodesics in BST geometries). Hence, for these naked singularity backgrounds, the $1S$ and $2S$ levels of hydrogen will receive gravitational corrections, contrary to the situation for black hole backgrounds.

We have calculated this shift and find that for radial geodesics, it can be large near the singularity for JNW space-times and for small radial distances for BSTs. We also calculated the shifts in the energy of some of the other states listed in [7] [Eqs. (6.1)–(6.23) of that paper] and find that in general, gravitational effects in JNW and BST backgrounds will be large only near the naked singularity, for radial geodesics.

We also calculated the energy shifts for circular geodesics and find that for JNW backgrounds, shifts in the hydrogen atom spectrum are qualitatively similar to those in Schwarzschild backgrounds; i.e., they become large only near the photon sphere [a result that is evident for the Schwarzschild geometry from Eqs. (6.15)–(6.23) of [7]] or near the naked singularity if the photon sphere is absent. The second situation is more interesting as it allows for stable orbits, as we have seen in Sec. II D. For BSTs, these are large only near the central singularity.

To conclude, we have presented a comprehensive GR analysis of effective magnetic fields seen by fermions in geodesic motion in curved space-times. Our results complement and add to the existing literature on the subject. We show evidence of large magnetic fields induced by gravity near a very massive gravitating object or near the center of a galaxy. We have also demonstrated qualitative differences in magnetic field, depending on the nature of space-time. Experimental signatures of these effects in futuristic experiments may be important to analyze.

ACKNOWLEDGMENTS

It is a pleasure to thank Kaushik Bhattacharya for very helpful discussions.

APPENDIX A

The nonzero components of the Riemann tensor in Fermi normal coordinates for circular geodesics in the background of Schwarzschild black hole (at $\theta = \pi/2$) are listed below. These also appear in [20].

$$
\begin{aligned}
R_{0101} &= \frac{r + 3(r - R_S)\cos(2\delta\phi)}{2r^3(2r - 3R_S)} R_S, \\
R_{0103} &= \frac{3R_S(r - R_S)}{2r^3(2r - 3R_S)} \sin(2\delta\phi), \\
R_{0113} &= -\frac{3R_S\sqrt{R_S(r - R_S)}}{\sqrt{2}r^3(2r - 3R_S)} \cos(\delta\phi), \\
R_{0202} &= -\frac{R_S}{r^2(2r - 3R_S)}, \\
R_{0212} &= \frac{3R_S\sqrt{R_S(r - R_S)}}{\sqrt{2}r^3(2r - 3R_S)} \sin(\delta\phi), \\
R_{0303} &= \frac{r - 3(r - R_S)\cos(2\delta\phi)}{2r^3(2r - 3R_S)} R_S, \\
R_{0223} &= -R_{0113}, \qquad R_{0313} = -R_{0212}, \\
R_{1212} &= -R_{0303}, \qquad R_{1223} = -R_{0103}, \\
R_{1313} &= -R_{0202}, \qquad R_{2323} = -R_{0101},
\end{aligned}
$$

where $R_S = \frac{2GM}{c^2}$, and $\delta = \sqrt{1 - \frac{3R_S}{2r}} = \sqrt{1 - \frac{3GM}{c^2 r}}$. In Fermi normal coordinates, it is easy to check that $R_{00} = 0$.

APPENDIX B

The nonzero components of Riemann tensor in Fermi normal coordinates for circular geodesics in the background of Bertrand space-time (at $\theta = \pi/2$) are listed below:

$$
\begin{aligned}
R_{0101} &= \alpha\beta^2 \frac{Dr + (\alpha + 3Dr)\cos 2\phi}{2r^2(\alpha + Dr)(\alpha + 2Dr)}, \\
R_{0103} &= \alpha\beta^2 \frac{(\alpha + 3Dr)\sin 2\phi}{2r^2(\alpha + Dr)(\alpha + 2Dr)}, \\
R_{0113} &= -\frac{\alpha^{3/2}\beta^2(\alpha + 4Dr)\cos\phi}{r^2(2(\alpha + Dr))^{3/2}(\alpha + 2Dr)}, \\
R_{0202} &= -\frac{\alpha}{r^2(\alpha + 2Dr)}, \\
R_{0212} &= \frac{\sqrt{\alpha}(\alpha(2 - \beta^2) + 2Dr(1 - \beta^2))\sin\phi}{r^2\sqrt{2(\alpha + Dr)}(\alpha + 2Dr)}, \\
R_{0223} &= \frac{\sqrt{\alpha}(\alpha(2 - \beta^2) + 2Dr(1 - \beta^2))\cos\phi}{r^2\sqrt{2(\alpha + Dr)}(\alpha + 2Dr)}, \\
R_{0303} &= \alpha\beta^2 \frac{Dr - (\alpha + 3Dr)\cos 2\phi}{2r^2(\alpha + Dr)(\alpha + 2Dr)}, \\
R_{0313} &= -\frac{\alpha^{3/2}\beta^2(\alpha + 4Dr)\sin\phi}{r^2(2(\alpha + Dr))^{3/2}(\alpha + 2Dr)}, \\
R_{1212} &= \frac{\beta^2(\alpha + 2Dr)(3\alpha + 2Dr) - 4(\alpha + Dr)^2}{2r^2(\alpha + Dr)(\alpha + 2Dr)} \sin^2\phi,
\end{aligned}
$$

$$R_{1223} = \frac{\beta^2(\alpha+2Dr)(3\alpha+2Dr) - 4(\alpha+Dr)^2}{4r^2(\alpha+Dr)(\alpha+2Dr)} \sin 2\phi,$$

$$R_{1313} = \frac{\alpha^2\beta^2(\alpha+4Dr)}{4r^2(\alpha+Dr)^2(\alpha+2Dr)},$$

$$R_{2323} = \frac{\beta^2(\alpha+2Dr)(3\alpha+2Dr) - 4(\alpha+Dr)^2}{2r^2(\alpha+Dr)(\alpha+2Dr)} \cos^2\phi.$$

For this space-time, it can be checked that in Fermi normal coordinates,

$$R_{00} = -\frac{\alpha(\alpha+Dr(1-\beta^2))}{r^2(\alpha+Dr)(\alpha+2Dr)}.$$

[1] S. Weinberg, *Gravitation and Cosmology* (John Wiley & Sons, New York, 1972).
[2] B. Mashhoon, arXiv:gr-qc/0311030.
[3] W. de Sitter, Mon. Not. R. Astron. Soc. **77**, 155 (1916).
[4] C. W. F. Everitt *et al.*, Phys. Rev. Lett. **106**, 221101 (2011).
[5] L. Parker, Phys. Rev. D **22**, 1922 (1980).
[6] L. Parker, Phys. Rev. Lett. **44**, 1559 (1980).
[7] L. Parker and L. O. Pimentel, Phys. Rev. D **25**, 3180 (1982).
[8] R. Bluhm and V. A. Kostelecky, Phys. Rev. Lett. **84**, 1381 (2000).
[9] See the official Web site at http://www.npl.washington.edu/eotwash/.
[10] S. Mohanty, B. Mukhopadhyay, and A. R. Prasanna, Phys. Rev. D **65**, 122001 (2002).
[11] U. Debnath, B. Mukhopadhyay, and N. Dadhich, Mod. Phys. Lett. A **21**, 399 (2006).
[12] V. A. Kostelecky and C. D. Lane, J. Math. Phys. (N.Y.) **40**, 6245 (1999).
[13] B. Mashhoon and Y. N. Obukhov, Phys. Rev. D **88**, 064037 (2013).
[14] F. K. Manasse and C. W. Misner, J. Math. Phys. (N.Y.) **4**, 735 (1963).
[15] D. Dey, K. Bhattacharya, and T. Sarkar, Phys. Rev. D **87**, 103505 (2013).
[16] D. Dey, K. Bhattacharya, and T. Sarkar, Phys. Rev. D **88**, 083532 (2013).
[17] R. Bluhm, V. A. Kostelecky, and C. D. Lane, Phys. Rev. Lett. **84**, 1098 (2000).
[18] C.-M. Claudel, K. S. Virbhadra, and G. F. R. Ellis, J. Math. Phys. (N.Y.) **42**, 818 (2001).
[19] R. A. Breuer, P. L. Chrzanowski, H. G. Hughes III, and C. W. Misner, Phys. Rev. D **8**, 4309 (1973).
[20] P. Collas and D. Klein, Gen. Relativ. Gravit. **39**, 737 (2007).
[21] A. Dey, P. Roy, and T. Sarkar, arXiv:1303.6824.
[22] V. Perlick, Classical Quantum Gravity **9**, 1009 (1992).
[23] H. Goldstein, *Classical Mechanics* (Narosa Publishing House, New Delhi, 1993), 2nd ed.
[24] J. F. Navarro, C. S. Frenk, and S. D. M. White, Astrophys. J. **462**, 563 (1996).
[25] L. Hernquist, Astrophys. J. **356**, 359 (1990).